Multistability and chaos in a spring-block model

V. B. Ryabov* and H. M. Ito
Seismology and Volcanology Research Department, Meteorological Research Institute, Nagamine 1-1, Tsukuba-shi, Ibaraki-ken, 305, Japan

(Received 3 January 1995; revised manuscript received 27 June 1995)

A simple spring-block model with two degrees of freedom capable of producing chaotic dynamics is studied. The stability properties of fixed points and symmetry properties of solutions are analyzed. Frequency-entrained oscillations are investigated by means of an averaging procedure, in the vicinity of a principal resonance. An approximate analytical condition of asymmetric attractors arising, which can be used as a precursor of the appearance of chaotic motions, is derived from the analysis of the fixed points of averaged equations. Multistability of the averaged system is studied in detail and is shown to be typical for the present model. Extensive computer experiments carried out within a broad range of control parameters demonstrate statisfactory agreement between theoretical predictions and numerical simulations. The calculated results are given in the form of two-parameter bifurcation diagrams, along with phase portraits of different coexisting attractors. Many features, characteristics of nonlinear oscillators, were observed, including period-doubling cascades, hysteresis, intermittency, and crises of chaotic attractors. The system is strongly multistable in the sense that usually a regular attractor coexists with a chaotic or quasiperiodic one. In this work we use a modified velocity-weakening friction law that admits the presence of creeping motion. The introduction of a small region of creeping motion into the velocity-friction relation is demonstrated to bring no principally new phenomena. Chaotic areas in control parameter space, however, broaden with the increase in the size of the creeping region.

PACS number(s): 05.45.+b

I. INTRODUCTION

In this paper we concentrate on one particular model with two degrees of freedom. The system belongs to the class of spring-block models with the velocity-weakening friction law, which have been used for a long time as deterministic simulators of earthquakes [1,2]. It was demonstrated recently that the models of this class can reproduce the well-known Gutenberg-Richter magnitude-frequency relation for earthquakes. In a series of papers by Carlson and co-workers [3–6] a detailed numerical study of the large system, having many degrees of freedom, has been carried out. It was shown, in particular, that without any spatial inhomogeneity and external noises a large variety of events with different sizes occurs in this system. The events of comparatively small magnitude obey the power law with an exponent close to unity, whereas the large events that are responsible for almost all energy release are much more frequent than can be expected from a simple extrapolation of the power law to larger magnitudes. The interrelation between small and large events was also investigated in order to provide a technique for testing and fine tuning the earthquake prediction algorithms [3,7–9].

The purpose of our study is to fill the gap that exists in the current knowledge of this class of models. On the one hand, many results have been accumulated, concerning various types of behavior observed in many-block simulations [3–18]. On the other hand, surprisingly little is known about the basic element of all these studies: the two-degree-of-freedom two-block model. At the same time, it is clear that some of the features exhibited by these large systems [11,12,17,18] may originate from the properties of their small subsystems consisting of few blocks only.

Another important motivation for the present work is that the system studied possesses a peculiar type of nonlinearity, with discontinuity in the friction law. This nonanalytic behavior of the friction force-velocity relation requires different differential equations to be used for defining the dynamics in different parts of the phase space. This type of dynamical systems, being of significant interest for applications, seems to be almost unexplored so far.

It was shown in [19] that this system can produce asymmetric regular patterns, thus leading to the conclusion about the possibility for nonlinear dynamics being responsible for the formation of a complex space-time distribution of earthquakes. Chaotic behavior was also detected in the analogous system with an asymmetric friction law [20]. However, the conclusion of [20] about spatial inhomogeneity as a necessary condition of chaos arising seems inconsistent with the results from the theory of nonlinear oscillations [21,22] since it was established that the symmetry does not forbid chaos. In con-

*On leave from the Institute of Radio Astronomy, 4 Krasnoznamennaya St., 310002 Kharkov, Ukraine.

trast, under certain conditions, the asymmetry of coupled oscillators may lead to the regularization of their motion [22].

In this article the study of the two-degree-of-freedom system with velocity-weakening friction is performed both analytically and numerically. The initial problem was taken in a form similar to that in [19], but with the friction law used in [4,20]. To our knowledge, the chaotic behavior has not been detected yet in this system without introduction of any spatial inhomogeneity. We have found a rich variety of possible dynamics, including chaos, and investigated the properties of the system under the variation of control parameters.

The main analytical tool we exploited for predicting the appearance of asymmetric dynamical patterns, which may be used as precursors of chaos in this system, was the averaging technique [23]. It permitted us to study the interrelation between some of the possible periodic regimes and helped in understanding the basic regularities underlying the behavior of the system.

It has also turned out that the symmetry properties of the equations play an important role in the dynamics, leading to the "strong" multistability. This means that the chaotic behavior was always observed to be accompanied by a regular motion, i.e., typically, the strange attractor coexisted with the periodic one in the phase space. Depending on the initial conditions, the system may evolve either chaotically or periodically, which is not surprising since it is a typical phenomenon observed in many studies of nonlinear oscillators [21,22,24]. The importance of this property for the present case consists in the fact that it seems to be preserved in numerical simulation with many-degree-of-freedom systems [4]. It was reported in [4] that zero initial conditions always led to a periodic behavior, while the random ones resulted in the now well-known irregular spatio-temporal patterns.

We have also studied the influence of a small area of creeping motion in the friction law on possible dynamics. Such an area is presumably a necessary component of any realistic friction law [25], but it has hardly been investigated yet. In the control parameter area under investigation the system demonstrated almost no essential difference for the cases when the creeping motion was present or absent, in the sense that no essentially new types of dynamics appear with the introduction of the small creeping region.

Finally, we have detected numerically a chaotic regime reminiscent of the irregular behavior of the large, many-degree-of-freedom system. We suppose that this regime may be especially important for the modeling of earthquake dynamics. A similar one was also reported in [20] for the system with an asymmetric friction law. It thus seems to be generic for the systems of coupled oscillators with velocity-weakening friction.

The article is organized as follows. In Sec. II the principal equations of two-block motion are discussed with particular attention given to the symmetry properties of the system and the stability of fixed points. Section III is devoted to the analysis of a single-oscillator system by means of an averaging procedure. The results obtained are generalized to the two-oscillator case in Sec. IV, where an approximate criterion of asymmetric limit cycles arising is derived. The description of the results of extensive numerical experiments and their comparison with theoretical predictions made on the basis of applying the method of averaging to the principal equations is the subject of Sec. V. In Sec. VI we summarize our main results.

II. BASIC EQUATIONS AND GENERAL PROPERTIES OF MOTION

The main object of our investigation it the system of two blocks of mass m (Fig. 1) coupled to each other by a linear spring of strength k_c and attached to a stationary plate by means of linear leaf springs of strength k_p. The bottom of each block is in contact with the rough plate, slowly moving with a constant speed α. This system may be considered as a simplest deterministic model of two-fault interactions. The dynamics of this system is described by the following ordinary differential equations for normalized coordinates x_1, x_2 measured from the rest positions of blocks, depending upon generalized parameters ω_0, κ:

$$\frac{d^2x_1}{dt^2}+\omega_0^2 x_1-\kappa x_2+F_{\rm fr}\left[\frac{dx_1}{dt}\right]=0\,,$$
$$\frac{d^2x_2}{dt^2}+\omega_0^2 x_2-\kappa x_1+F_{\rm fr}\left[\frac{dx_2}{dt}\right]=0\,, \tag{1}$$

where $\omega_0^2=k_p+k_c$ and $\kappa=k_c$.

The derivation of this system from Newtonian equations of motion is straightforward and may be found, for example, in [4,20]. Of the two parameters ω_0 and κ only one is essential. The remaining one can always be made equal to an arbitrary value by elementary scaling of coordinates and time. We, however, prefer to preserve at the present stage this form of equation because, from our point of view, it is more convenient for the subsequent analysis. The function $F_{\rm fr}(dx_i/dt)$ (hereinafter $i=1,2$) is the friction force depending only on the relative velocity of a block with respect to the moving plate. In our study we use the following form of the friction law (see Fig. 2):

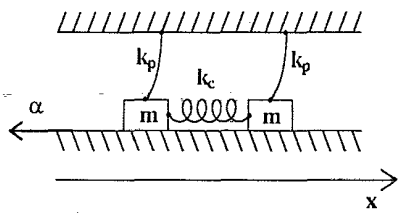

FIG. 1. The mechanical model studied.

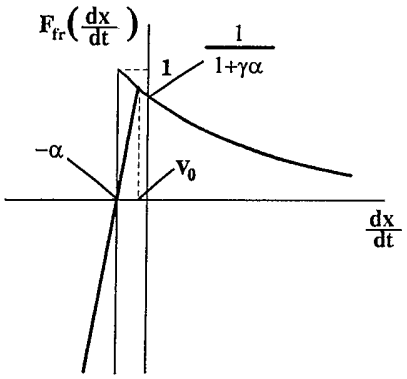

FIG. 2. Friction law in Eq. (1).

$$F_{\rm fr}\left[\frac{dx_i}{dt}\right]=\begin{cases} g\left[\alpha+\dfrac{dx_i}{dt}\right] & \text{at } \dfrac{dx_i}{dt}<v_0 \\ 1+\gamma\left[\alpha+\dfrac{dx_i}{dt}\right] & \text{at } \dfrac{dx_i}{dt}>v_0 \end{cases},$$

where (1′)

$$v_0=-\alpha+\frac{1}{\gamma}\left[\left[\frac{1}{4}+\frac{\gamma}{g}\right]^{1/2}-\frac{1}{2}\right].$$

The maximal magnitude of the friction without loss of generality is taken to be equal to unity $F_{\rm fr}(v_0)=1$. The parameter α is directly related to the speed of constant plate motion. The value of γ controls the degree of instability introduced by the velocity-weakening friction. The parameter g characterizes the creeping region where the friction force is chosen to be proportional to the relative velocity. At magnitudes of the velocity higher than a certain threshold value v_0 defining the width of the creeping area, the usually exploited functional form of friction law provides the instability necessary for stick-slip motion. If $g\to\infty$, we arrive at the well known [3–6] singular friction-velocity relation without creeping. The introduction in this work of a parameter g thus permits us to investigate the transition from the friction law with a singularity to the more physically relevant friction-velocity dependence.

The solution of nonlinear equations (1) cannot be found in closed form. However, some important information about possible oscillatory regimes can be deduced from the analysis of its fixed points. Rewriting the system in the standard form, we obtain four ordinary differential equations of first order

$$\begin{aligned} \frac{dz_1}{dt}&=z_2\ , \\ \frac{dz_2}{dt}&=-\omega_0^2 z_1+\kappa z_3-F_{\rm fr}(z_2)\ , \\ \frac{dz_3}{dt}&=z_4\ , \\ \frac{dz_4}{dt}&=-\omega_0^2 z_3+\kappa z_1-F_{\rm fr}(z_4) \end{aligned} \qquad (2)$$

It can be seen that the system (2) possesses two fixed points at $z_{2,4}=0$, $z_{1,3}=F_{\rm fr}(0)/(\kappa-\omega_0^2)$. Linearization of Eqs. (2) in the vicinity of these points gives the characteristic polynomial

$$[\lambda^2+F'_{\rm fr}(0)\lambda+\omega_0^2-\kappa][\lambda^2+F'_{\rm fr}(0)\lambda+\omega_0^2+\kappa]=0\ , \qquad (3)$$

where the stroke means differentiation with respect to velocity. Then, at $F'_{\rm fr}(0)<0$ both fixed points are unstable, and, hence, stick-slip motion occurs in this case. The following relation immediately follows from (2) and (3), which should always hold in order to provide the existence of self-sustained oscillations:

$v_0<0$ or, in other terms,

$$\alpha>\alpha_{\rm th}\equiv\frac{1}{\gamma}\sqrt{\tfrac{1}{4}+(\gamma/g)}-\tfrac{1}{2}\ . \qquad (4)$$

The expression (4) is equivalent to the condition of Hopf bifurcation to occur in the system. At the line in the control parameter space (CPS) defined by the equation $\alpha=\alpha_{\rm th}$ the real parts of the eigenvalues given by (3) change their sign, leading to the instability of fixed points and to arising of a limit cycle in the phase space.

Additional general information concerning possible solution types of the system (1) can be obtained from the analysis of its symmetry properties. It is easy to verify that Eqs. (1) are invariant with respect to the change of coordinates: $x_1\leftrightarrow x_2$. This implies that, generally speaking, two types of attractors could be expected to occur in the phase space. The first one, which we will refer to as symmetric, corresponds to the situation when the trajectories in subspaces (z_1,z_2) and (z_2,z_4) evolve in a sense alike, producing similar phase space patterns. The second type of motion, we refer to as asymmetric, leads to different phase space portraits in the pointed out subspaces. The asymmetric attractors always appear in pairs, which is an apparent consequence of the invariance of Eqs. (1) with respect to the transformation $x_1\leftrightarrow x_2$. As will be shown below, the symmetric periodic attractors as a rule exist in the phase space, at almost any values of control parameters, and, thus, may be called superstable, contrary to the asymmetric ones. The motion of the last type, existing only in a restricted area of the CPS, plays an important role in the formation of complicated dynamics. The largest region of chaotic behavior found numerically (see Sec. V) is associated with arising of asymmetric attractors. So, the appearance of asymmetric periodic attractors may be used as a precursor of chaos in this particular system.

Another important property of the system (1) is the presence of two physically important time scales, depending on the interrelation between parameters ω_0, κ, γ, and α. Note, that parameters ω_0, κ and γ mainly define the characteristic time T_r of energy release (or slipping motion) in the system, while the parameter α controls the energy accumulation (or loading) time T_a in the "stick" phase of motion. Therefore, the properties of solutions have to be different for the cases $T_r\ll T_a$, which corresponds to $\alpha\ll 1$, and $T_r\gg T_a$, $\alpha\leq 1$. It will be demonstrated numerically (Sec. V) and follows from some analytical considerations (Sec. III) that the former case,

which is of special importance for earthquake modeling, occurs in a comparatively small area in the CPS where the system evolves in a highly nonlinear regime. In the latter case, the typical phenomena observed should be similar to the ones characteristic of other oscillatory systems (see, for example, the results reported in [21,22,26,27] for coupled oscillators of different types).

The distinctive properties of the present system are (i) its nontrivial type of nonlinearity and (ii) the uniformity, i.e., the equivalence of individual oscillators, that manifests itself in equal values of parameters ω_0 and κ for both oscillators constituting the system (1). Various resonances are expected to occur under the variation of control parameters, demonstrating such phenomena as frequency entrainment, hysteresis with characteristic jumps of solutions from one branch to another, period doublings, chaos, and intermittency. The results of numerical experiments given below demonstrate the presence of all pointed out regimes and indicate that the two types of motion with different characteristic time scales are closely related and there is a smooth transition between them.

If the nonlinearity is small, the well-known averaging procedure is usually applied for the study of periodic motions, i.e., limit cycles. In a typical situation (see [28] for examples), when some nonlinear system is analyzed, the degree of nonlinearity is totally defined by a single parameter, which is supposed to be small for the averaging to apply. The peculiarity of the system (1) consists in the fact that there is no such parameter that could control nonlinearity. Instead, the magnitudes of α, γ, and g, which determine the friction law, are responsible for nonlinear effects. To proceed, we will assume that coupling κ and the maximal magnitude of friction $F_{\rm fr}(v_0)$ are small for the time being. This permits us to formally perform averaging and thus get some information about possible oscillatory regimes. However, it should be kept in mind that the results obtained will be valid only in the parameter region where the solution is sufficiently close to the harmonic oscillation. We suppose that the strong nonlinearity manifests itself in this system when the conditions $\alpha \ll 1$, $g \gg 1$, or $\gamma \gg 1$ hold. In any case, like in any similar problem, the predictions made on the basis of averaging are only approximate ones and must be verified numerically.

The theoretical analysis will be carried out in two steps. First, the one-degree-of-freedom single-oscillator system will be considered. The formulas obtained will be used in the second step for the analysis of the two-degree-of-freedom system. Then the numerical study will be performed in order to verify the analytical predictions made.

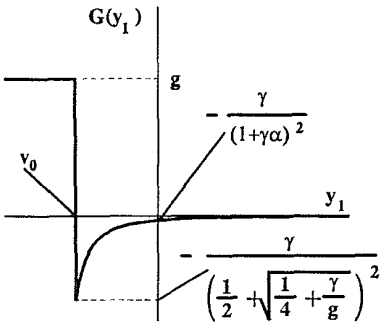

FIG. 3. Friction potential function in Eqs. (5) and (8).

III. ONE-BLOCK SYSTEM

If we set the coupling parameter κ in (1) equal to zero, the system splits into two independent equations of single oscillators. For the sake of convenience, the following variables are introduced: $y_1 = dx/dt$ and $y_2 = d^2x/dt^2$, where x is either x_1 or x_2. This transformation permits us to shift the position of the fixed point to zero without any complication of the form of the equations. The system for the single oscillator in these variables looks like

$$\frac{dy_1}{dt} = y_2 ,$$

$$\frac{dy_2}{dt} = -\omega_0^2 y_1 - G(y_1) y_2 ,$$

where

$$G(y_1) = \begin{cases} g & \text{at } y_1 < v_0 \\ -\dfrac{\gamma}{[1+\gamma(\alpha+y_1)]^2} & \text{at } y_1 > v_0 . \end{cases} \tag{5}$$

The plot of the function $G(y_1)$ is depicted in Fig. 3. This system possesses a fixed point at $y_1 = y_2 = 0$ that is unstable if (4) holds and stable otherwise. It is clear from physical considerations (restricted amplitude of block motion) and can be easily shown analytically that the solution of (5) is bounded. Then, since the system (5) is two dimensional, the only alternative to a stable fixed point is a limit cycle that should coexist in the phase space with the unstable fixed point. To derive its amplitude we will apply the averaging procedure in its standard way [23].

We will seek the solution in the form $y_1 = a(\tau)\cos\Psi(t,\tau)$, where $\Psi(t,\tau) = \omega_0 t + \theta(\tau)$ and τ is slow time. Then the following equations for the slow amplitude and phase of the oscillation are derived by averaging over the "fast" period $T = 2\pi/\omega_0$:

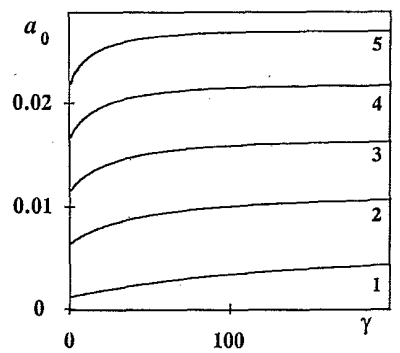

FIG. 4. Amplitude of the limit cycle in system (5) [coordinate of the fixed point in (6)] at $g = 260, \alpha = 0.05$ (curve 1), 0.01 (curve 2), 0.015 (curve 3), 0.02 (curve 4), and 0.025 (curve 5).

$$\frac{da}{d\tau}=\frac{a}{\pi}\left[\gamma I(a)-\frac{g}{2}\left[\pi-\xi(a)+\frac{1}{2}\sin[2\xi(a)]\right]\right], \qquad \frac{d\theta}{d\tau}=0 . \tag{6}$$

Here

$$\xi(a)=\begin{cases}\arccos\dfrac{v_0}{a} & \text{if } a>-v_0\\ \pi & \text{if } 0<a<-v_0\end{cases}, \tag{6a}$$

$$I(a)=\int_0^{\xi(a)}\frac{\sin^2\Psi\,d\Psi}{[1+\gamma(\alpha+a\cos\Psi)]^2} . \tag{6b}$$

The value of the integral $I(a)$ can be found analytically and has the form

$$I(a)=\begin{cases}\dfrac{1}{d^2}\left\{-\xi(a)+\dfrac{d\sin\xi(a)}{1+\gamma(\alpha+v_0)}+\dfrac{c}{\sqrt{c^2-d^2}}\left[\dfrac{\pi}{2}+\arctan\left[-\dfrac{d+c\cos\xi(a)}{\sqrt{c^2-d^2}\sin\xi(a)}\right]\right]\right\}\\ \quad \text{at } -v_0<a<\alpha+\dfrac{1}{\gamma}\\ \dfrac{1}{d^2}\left\{-\xi(a)+\dfrac{d\sin\xi(a)}{1+\gamma(\alpha+v_0)}+\dfrac{c}{\sqrt{d^2-c^2}}\ln\left[\dfrac{d+c\cos\xi(a)+\sqrt{d^2-c^2}\sin\xi(a)}{1+\gamma(\alpha+v_0)}\right]\right\}\\ \quad \text{at } a>\alpha+\dfrac{1}{\gamma},\end{cases}$$

where $d=\gamma a$ and $c=1+\gamma\alpha$.

The fixed points of (6) represent periodic orbits in the original equations (5). Their position can be found by solving the nonlinear algebraic equation by equating the right-hand side of (6) to zero. Apart from the trivial solution $a=0$, there is always another root a_0 corresponding to the stable oscillation with nonzero amplitude, found from the equation

$$\gamma I(a)=\frac{g}{2}P(a) , \tag{7}$$

where

$$P(a)\equiv\pi-\xi(a)+\tfrac{1}{2}\sin[2\xi(a)] .$$

In Fig. 4 the values of a_0 derived numerically by solving (7) are depicted vs γ at different magnitudes of α. As could be expected, the amplitude of the limit cycle grows with γ. This property could be easily understood if we take into consideration that γ controls the instability degree of the system.

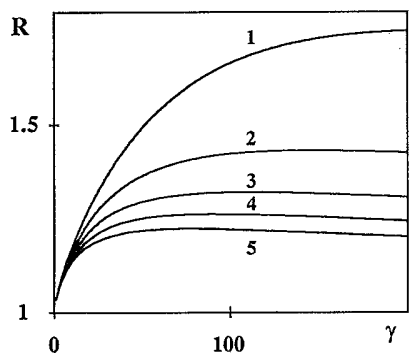

FIG. 5. Ratio $-a_0/v_0$ vs γ at $g=260$; $\alpha=0.005$ (curve 1), 0.01 (curve 2), 0.015 (curve 3), 0.02 (curve 4), and 0.025 (curve 5).

It is worth noting also that this stationary oscillation has the amplitude of the order of $-v_0$ and cannot be less than this value. This follows from the structure of Eq. (6) for the amplitude and Fig. 3. Since $I(a)$ and $P(a)$ are non-negative, the positive parameters g and γ are responsible for the process of energy balance in the system (6), the former defining the dissipation rate and the latter being responsible for the instability rate or amplitude increase. (Note that the amplitude of the oscillation increases during the slip phase of motion and decreases when the block is stuck.) Suppose that at the initial time moment the velocity and acceleration of the block are close to zero. Then, since the fixed point at the origin is unstable, the amplitude of the oscillation will increase to the value $-v_0$, where the energy begins to dissipate with the rate defined by the parameter g. This rate is rather high (the greater g value, the higher the rate) because the creeping area is small and, consequently, the steady state amplitude will be reached at some value not considerably larger than $-v_0$. This fact is illustrated in Fig. 5, where the dependences of the ratio $R\equiv-a_0/v_0$ upon γ at different α are given.

From this results a very important conclusion that the smaller the velocity of constant plate motion, the smaller the amplitude of oscillations excited in this system. This inference imposes a strong limitation on the ratio of time scales responsible for stick and slip phases of motion, making them about the same order of magnitude. The estimate of T_a/T_r can be obtained if we assume that the characteristic time of the slip phase is about the value of the "fast" period over which the averaging has been applied, i.e., $T_r\cong 2\pi/\omega_0$, whereas the corresponding time scale of the stick phase is not greater than the duration of the motion with constant velocity $-v_0$ between two con-

secutive stick positions of the block defined by

$$T_a \leq -\frac{\Delta x_{\max}}{v_0},$$

where $\Delta x_{\max}=2a_0/\omega_0$ since $x=\int y_1 dt=\int a_0\cos(\omega_0 t+\theta_0)dt$.

Within this approximation $T_a/T_r \leq -a_0/v_0 \cong \text{const}$ under the variation of γ at fixed α and the ratio increases with a decrease in α (see, Fig. 5). Hence it seems impossible to find oscillatory regimes with considerably different time scales when the nonlinearity is small ($\alpha \leq 1$ and $\gamma \ll 1$) and the averaged system describes properly the behavior of solutions. The well separated characteristic times have to appear in a strongly nonlinear area of control parameters, i.e., at very small α and large γ. So, by this expediency, the study of the single-block system carried out here permits us to specify the control parameters area where the model can produce the behavior in some sense similar to the dynamics of faults.

The general observation following from the analysis of a single-block oscillator is that the averaging technique can be used for the analysis of oscillatory regimes in this system and its application leads to results that qualitatively do not defy the common sense. However, it should be clear that quantitative characteristics of the oscillation calculated from the averaged system, such as, for example, the amplitude and period of a limit cycle, may differ significantly from the true ones in the strongly nonlinear part of CPS.

IV. TWO-BLOCK SYSTEM

Now we will apply the averaging technique to the system of two oscillators described by the equations written in the form of (5), i.e., in terms of the velocity and acceleration of two blocks

$$\begin{aligned}
\frac{dy_1}{dt}&=y_2,\\
\frac{dy_2}{dt}&=-\omega_0^2 y_1+\kappa y_3-G(y_1)y_2,\\
\frac{dy_3}{dt}&=y_4,\\
\frac{dy_4}{dt}&=-\omega_0^2 y_3+\kappa y_1-G(y_3)y_4.
\end{aligned} \tag{8}$$

This system is obtained by the differention of (2) with respect to time. The function $G(y_i)$ is similar to the one in (5) and its plot is given in Fig. 3. Applying the procedure used in Sec. III, we seek the solution in the form $y_1=a_1(\tau)\cos\Psi_1(t,\tau)$, $y_2=a_2(\tau)\cos\Psi_2(t,\tau)$, where $\Psi_1(t,\tau)=\omega_0 t+\theta_1(\tau)$, $\Psi_2(t,\tau)=\omega_0 t+\theta_2(\tau)$. The averaging leads to the system of equations

$$\begin{aligned}
\frac{da_1}{d\tau}&=\frac{a_1}{\pi}\left\{\gamma I(a_1)-\frac{g}{2}[\pi-\xi_1(a_1)+\sin\xi_1(a_1)\cos\xi_1(a_1)]\right\}+\frac{\kappa\sin\theta}{2\omega_0}a_2,\\
\frac{da_2}{d\tau}&=\frac{a_2}{\pi}\left\{\gamma I(a_2)-\frac{g}{2}[\pi-\xi_2(a_2)+\sin\xi_2(a_2)\cos\xi_2(a_2)]\right\}-\frac{\kappa\sin\theta}{2\omega_0}a_1,\\
\frac{d\theta}{d\tau}&=\frac{\kappa}{2\omega_0}\left[\frac{a_2}{a_1}-\frac{a_1}{a_2}\right]\cos\theta,
\end{aligned} \tag{9}$$

where $\theta=\theta_2-\theta_1$, $a_i\cos\xi_i=v_0$, and $I(a_i)$ are given by (6b) if we substitute a_i,ξ_i,Ψ_i instead of a,ξ,Ψ.

Equating the right-hand sides of (9) to zero, we obtain the system of nonlinear algebraic equations for the coordinates of fixed points a_1^*,a_2^*,θ^*. It is clear from the form of the third equation of (9) that there are two types of fixed points in this averaged system: (i) $a_1^*=a_2^*\equiv a^*$, $\theta^*=0$ or π and (ii) $a_1^*\neq a_2^*$, $\theta^*=\pm\pi/2$. Hereafter, we will refer to these situations as case (i) and (ii). They correspond, respectively, to symmetric and asymmetric trajectories in the system (7) (see Sec. II for the definition of symmetries). It should be stressed that for a definite combination of control parameters these fixed points coexist, which brings into existence the multistability of the system. This property is of substantial importance because it is responsible for most of the complexity of the dynamics, appearing as the variety of possible oscillatory motions and transitions between them.

Let us now consider both cases separately.

Case (i). Actually, there are two types of symmetric limit cycles in the system (8), which differ in the position of the associated fixed points in (9) ($\theta^*=0$ or π). Following [22], we will refer to them, respectively, as "in-phase" and "out-of-phase" solutions. Their amplitudes a^* are defined by exactly the same equation as (7) and the stability is determined by the variational equations with the characteristic polynomial

$$\left[\frac{dH(a^*)}{da}-\lambda\right]\left[\lambda^2-\lambda\frac{dH(a^*)}{da}+\frac{\kappa^2}{\omega_0^2}\right]=0. \tag{10}$$

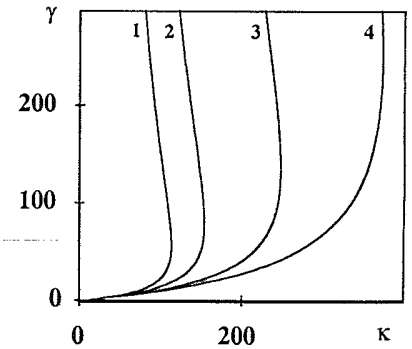

FIG. 6. Lines of saddle-node bifurcation of asymmetric fixed points in the averaged system (9), delimiting the area of asymmetric attractors existence. The parameters are $g=260$ and $\alpha=0.03$ (curve 1), 0.02 (curve 2); 0.01 (curve 3), and 0.005 (curve 4).

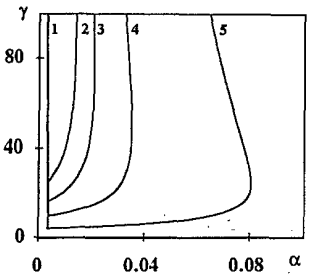

FIG. 7. Position of Hopf bifurcation in system (2) (curve 1) and lines corresponding to saddle-node bifurcation of asymmetric fixed points in averaged equations (9) (curves 2–5). The parameters are $g=260$ and $\kappa=200$ (curve 2), 150 (curve 3), 100 (curve 4), and 50 (curve 5).

Note that this equation is the same for both fixed points. This immediately leads to the conclusion that the linear stability properties of both symmetric attractors are identical. Moreover, from the results obtained in Sec. III for the single-block oscillator it follows that solutions of this type exist at almost any value of control parameters and are always stable. This means that under any combination of parameters there exist two stable limit cycles in the phase space of the system (8) [or (2), which is equivalent to (8)], at least in the region where Eqs. (9) describe properly the solutions of (8). In Sec. V it will be demonstrated that the results of numerical experiments are in good agreement with this theoretical prediction. In particular, numerical integration of the system (2) indicates the presence of "superstable" symmetric attractors in the whole region of control parameters that was investigated by us. The coexistence of in- and out-of-phase attractors in the phase space causes additional difficulty for the numerical analysis since it results in sudden jumps of phase trajectory between these regimes, as a rule accompanied by hysteresis.

Case (ii). The asymmetric case is more complicated for analytical treatment, first of all because of the nontrivial character of the $I(a_i)$ dependence. Nevertheless, it appears possible to specify the region in the CPS where a solution of this type exists. As shown in the Appendix, this problem associated with solving the system of nonlinear algebraic equations for the coordinates of fixed points in the phase space of the system (9) can be reduced to the analysis of the relation

$$\frac{4\omega_0^2\gamma}{\pi^2\kappa^2}I(-v_0)\left\{\gamma I(W_0)-\frac{g}{2}[\pi-\xi(W_0)+\sin\xi(W_0)\cos\xi(W_0)]\right\}\geq -1\ , \quad (11)$$

where $W_0=-(2\omega_0 v_0/\pi\kappa)\gamma I(-v_0)$; $\xi(W_0)$ is defined by $W_0\cos\xi(W_0)=-v_0$, and

$$I(-v_0)=\frac{\pi}{\gamma^2 v_0^2}\left[\frac{1+\alpha\gamma}{\sqrt{(1+\alpha\gamma)^2-\gamma^2 v_0^2}}-1\right].$$

If only symmetric attractors are present, i.e., only stable limit cycles together with unstable foci exist in the

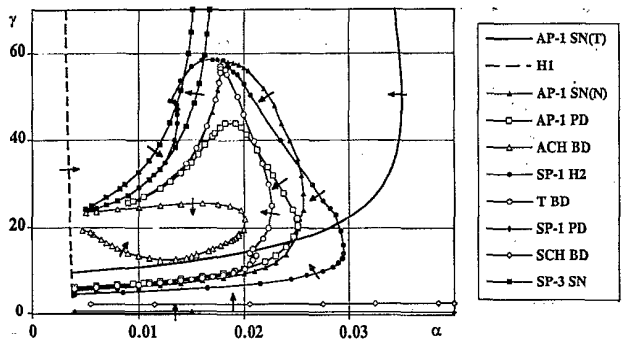

FIG. 8. Bifurcation diagram of system (2) at $g=260$; $\kappa=100$. Arrows indicate the direction of parameter change when bifurcations described in the text occur. The heavy solid and dotted lines are calculated from formulas (11) and (4), respectively; other curves are obtained numerically. AP-1 SN(T), saddle-node (theoretical) bifurcation leading to the rise of asymmetric fixed points in the system (9); AP-1 SN(N), saddle-node (numerical) bifurcation of asymmetric limit cycles arising in the system (2); H1, primary Hopf bifurcation; AP-1 PD, first period doubling of asymmetric periodic orbits; ACH BD, breakdown of the chaotic attractor originating from asymmetric solutions; SP-1 H2, secondary Hopf bifurcation of a symmetric period-1 orbit, with a two-dimensional torus appearing; TBD, torus breakdown; SP-1 PD, first period doubling of the symmetric period-1 attractor; SCH BD, breakdown of the chaotic attractor originating from the symmetric orbit; SP-3 SN, period-3 saddle-node bifurcation.

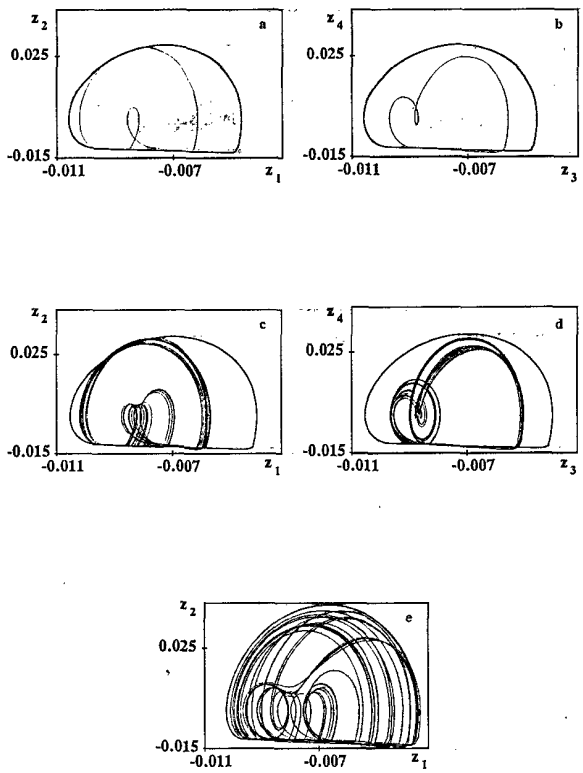

FIG. 9. Evolution of phase portraits of asymmetric attractors (thin lines) and coexisting symmetric in-phase solutions with a change in γ at $\alpha=0.015$; $\gamma=8.0$ (a) and (b), 9.0 (c) and (d), 12.0 (e).

phase space, it is insufficient for chaos to arise. The source of complexity in nonlinear dynamical systems is saddle-type unstable orbits that typically arise together with additional stable periodic solutions. In order to demonstrate how this occurs in the given system, let us consider its characteristic equation

$$\left[\mp\frac{\kappa}{2\omega_0^2}\left[\frac{a_2^*}{a_1^*}-\frac{a_1^*}{a_2^*}\right]-\lambda\right] \times\left[\left[\frac{dH(a_1^*)}{da}-\lambda\right]\left[\frac{dH(a_2^*)}{da}-\lambda\right]+\frac{\kappa^2}{4\omega_0^2}\right]=0 . \tag{12}$$

It is clear from (12) that of the two fixed points of this type ($\theta^*=\pi/2$ or $-\pi/2$), at least one is unstable. Thus the prediction made for the appearance of asymmetric periodic attractors would be in essence the indication of the arising of unstable saddle orbits and associated complexity in the phase space.

Before proceeding to the numerical analysis of the system (2), we need to specify the region of interest where complicated dynamics is likely to occur. We suggest the use of the expression (11) for this purpose and solve it numerically in order to obtain the borderlines of existence of asymmetric attractors in the two-parameter sections of the CPS. This can be achieved by fixing two of the principal parameters (κ,g,α,γ) and solving Eq. (11) at different values of the remaining two. The results of such calculations at various combinations of parameters are given in Figs. 6 and 7. The curves correspond to the equality sign in (11) and the region of existence for the asymmetric solutions lies to the left of these curves. Together with these lines, in Fig. 7 the curve corresponding to the condition (4), i.e., the position of Hopf bifurcation, is also shown. The self-sustained oscillations exist to the right of this line. So the area of complicated dynamics is likely to exist between the curves defined by Eqs. (11) and (4). A straightforward way to check the predictions made is to solve numerically Eqs. (2), which is done in the next section.

V. NUMERICAL EXPERIMENTS

We integrated numerically the system (2) by the Runge-Kutta procedure of fourth order and studied the principal bifurcation phenomena that occur under the variation of control parameters. The continuation technique was used for tracking the lines of local bifurcations on two-dimensional cross sections of the CPS. Since we were interested only in the global features of this system, we restricted our study to the investigation of the oscillatory regimes that occupy significant areas in the CPS. Such extended regions were detected for various period-1 and period-3 frequency-entrained solutions, two-dimensional tori, and chaotic attractors of different types. We thus did not explore the abundant higher-order frequency entrainments and resonances on tori because of their seemingly insignificant influence on the global picture of the dynamics.

In order to distinguish between chaos and quasiperiodicity we calculated the largest characteristic Lyapunov exponent. This quantity may now be considered as a standard tool for detecting chaotic dynamics in nonlinear systems.

The majority of numerical results presented in this work were obtained at finite values of the parameter g, responsible for the character of the nonlinear friction law (1a). Such a choice for g makes nonsingular the dependence of friction force upon the velocity and so enables us to apply the standard technique of calculation for the Lyapunov exponent [29]. When studying the singular case, we applied only the analysis of phase portraits, two-dimensional projections of three-dimensional Poincaré cross sections, and the continuation technique, extrapolating the properties of the nonsingular system to the singular one. The general features of bifurcation diagrams seem to be preserved in the presence of singularity, as well as the typical scenarios of chaos arising and a general view of phase portraits.

In all our calculations we used the following value of natural frequency of oscillators: $\omega_0^2=201$. Out of the remaining four control parameters, α, γ, g, and κ, we fixed some two of them and considered the changes in the system's behavior under the variation of the remaining two.

Let us demonstrate first how the dynamics of this system depends upon the parameters determining the form of friction law. For this purpose we put $g=260$, $\kappa=100$ and study successively the transformation of asymmetric and symmetric attractors under the change in α and γ.

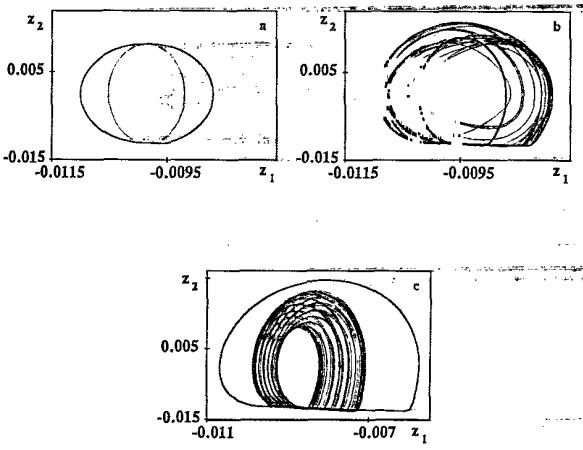

FIG. 10. Coexisting in- and out-of-phase symmetric attractors at $\alpha=0.015$; $\gamma=0.2$ (a), 2.0 (b), and 6.0 (c).

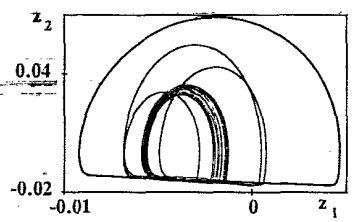

FIG. 11. Coexisting symmetric attractors: two-dimensional torus (thin line in the center of the plot), period-3 in-phase orbit (one-point line), and period-1 in-phase (two-point line) orbit. Parameter values: $\alpha=0.015$; $\gamma=50.0$.

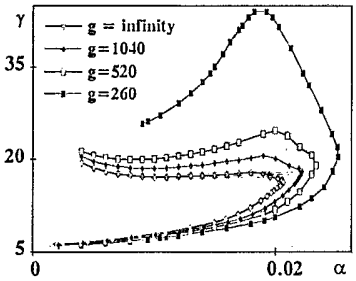

FIG. 12. First period-doubling lines of asymmetric attractors under the variation of g. $\kappa=100.0$.

The results of extensive numerical experiments are shown in Figs. 8–11 in the form of the bifurcation diagram and corresponding phase portraits of attractors. Throughout this section we use two two-dimensional projections in order to depict asymmetric attractors and a single one for the symmetric motions, being aware that the second projection looks exactly the same. It is also worth noting that under the variation of control parameters, attractors of different types change in certain respects independently, which manifests itself in a rather complicated pattern of bifurcation lines in Fig. 8. Thus, it should be kept in mind that different lines often correspond to different attractors. Another important peculiarity of this system is the "superstability" of symmetric attractors. This means that at any point of the CPS we explored there always existed at least one regular (periodic) stable symmetric solution.

The initial area for our study was chosen in accordance with Fig. 7, i.e., in the region where, as follows from the results of Sec. IV, asymmetric solutions must occur. In Fig. 8 the lines H1 and AP-1 SN(T), delimiting the area where asymmetric fixed points exist in the phase space of the system (9), correspond to curves 1 and 4 in Fig. 7, respectively. The arrows show the direction of change in the control parameters leading to the Hopf and saddle-node bifurcations, respectively.

The numerically obtained line AP-1 SN(N) indicates the position where asymmetric period-1 limit cycles arise in the phase space of the system (2). A comparison of the mutual arrangement of lines AP-1 SN(N) and AP-1 SN(T) in this diagram enables us to conclude that the quality of the prediction made on the basis of averaging may be considered as satisfactory, taking into account the approximate character of our theoretical analysis. An example of the asymmetric period-1 attractor is given in Figs. 9(a) and 9(b). Note that simultaneously with the pointed out orbit, another attractor [not shown in Figs. 9(a) and 9(b)], symmetric with respect to the transformation $x_1 \leftrightarrow x_2$, exists in the phase space.

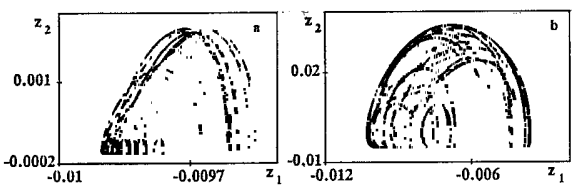

FIG. 13. Phase portraits of chaotic attractors at $g=\infty$, $\kappa=100$; $\gamma=14.5$, (a) $\alpha=6.25\times10^{-5}$ and (b) $\alpha=5.0625\times10^{-3}$.

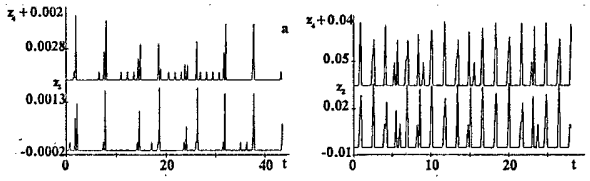

FIG. 14. Time profiles corresponding to the phase portraits of Fig. 13.

Our further experiments show that, when moving inside the area enclosed by the line AP-1 SN(N), the asymmetric limit cycles undergo period-doubling bifurcation (line AP-1 PD in Fig. 8) and become chaotic through subsequent period doublings. One of the coexisting strange attractors is depicted in Figs. 9(c) and 9(d). Under the change of control parameters towards the line ACH BD, both attractors first merge at symmetry increasing bifurcation (not shown) and then disappear at the ACH BD curve in the blue-sky catastrophe. In such a manner, when crossing the line ACH BD, a trajectory suddenly jumps to the coexisting symmetric period-1 in-phase attractor [see Figs. 9(a)–9(d)]. The symmetric strange attractor just before the catastrophe is given in Fig. 9(e).

Another chaotic motion area detected in our simulation is associated with a symmetric in-phase attractor. It occurs at a relatively small magnitude of the parameter γ and the threshold value γ_c of chaos arising is almost independent of α. An interesting feature of this regime is that even in the chaotic state, both oscillators constituting the system move almost identically, thus providing an example of synchronized chaos [30]. In order to give an illustration of the way this regime arises, we begin from the very low values of γ, where only symmetric periodic motions exist. Coexisting in- and out-of-phase periodic attractors are shown in Fig. 10(a). Under the increase of γ, the in-phase one undergoes the first period-doubling bifurcation at the line SP-1 PD of Fig. 8, with a subsequent transition to chaos through period doublings. The resulting synchronous strange attractor is depicted in Fig. 10(b) together with the remaining almost unchanged out-of phase period-1 orbit. After crossing the curve ACH BD, this chaotic attractor disappears in a blue-sky manner and the trajectory is attracted to the out-of-phase periodic solution.

The set of possible oscillatory regimes existing in the part of the CPS shown in Fig. 8 is not exhausted by periodic and chaotic motions only. The quasiperiodic attractor was also detected in our experiments within the area delimited by the lines SP-1 H2 and TBD. The crossing of the curve SP-1 H2 in the direction shown by the arrow results in secondary Hopf (or Neimark) bifurcation, when the stable out-of-phase symmetric attractor transforms into a two-dimensional torus [see Fig. 10(c)]. This torus exists in an extended area of the CPS and may coexist with different attractors mentioned above, including chaotic ones. Moreover, when approaching the line TBD, the torus itself transforms to a chaotic attractor through losing its smoothness. The simultaneous presence of quasiperiodic and chaotic motions in the phase

space makes the bifurcation pattern especially complicated in this area, mainly because of various resonances that occur on the torus. We, however, did not study these patterns in detail in the framework of the present paper.

Apart from the attractors already discussed, there exists another one, a period-3 solution. We calculated the position of the borderline for the period-3 regime, occupying a large area in the CPS, and depicted it as the SP-3 SN curve in Fig. 8. Figure 11 provides an illustration of this regime, where it coexists with a symmetric torus and periodic in-phase attractor.

The next step we made for understanding the general regularities of interrelation between different regimes in the system consisted in increasing the parameter g, which controls the width of creeping area in the friction law (1'). As an example, we produced Fig. 12, where we demonstrated how the chaos area delimited by the line AP-1 PD from Fig. 8 shrinks, remaining finite, when g tends to infinity.

Now we would like to return to the discussion of the problem concerning the ratio between time scales of stick and slip phases of motion. As demonstrated in Sec. III, the single-oscillator system "tends" to keep this quantity approximately constant, the decrease in α being the only way of separating the time scales. This property was observed to be preserved in the two-block system. In fact, almost all the attractors mentioned above, including chaotic ones, are characterized by a not very high value of this ratio, typically less than or equal to 10. The main cause of such behavior is presumably not the sufficiently low values of α used in many of our simulations. The restriction from below on α imposed by the relation (4) did not permit us to assign arbitrarily small values to this parameter, which is defined, in turn, by the finite magnitude of g. On the contrary, at g sufficiently large, we observed the chaotic regime with significantly separated time scales within the area delimited by the line AP-1 PD, in the region of $\alpha \ll 1$. This case corresponds to the strange attractor emerging as a result of period doublings from the asymmetric orbit. A phase portrait of such a regime is given in Fig. 13(a) and the corresponding time profile is depicted in Fig. 14(a). It is clearly seen that the behavior of the system consists of asynchronous small size slipping events, intermittent with synchronously occurring two-block movements. It is also evident that the characteristic time of slip phases is much smaller than the duration of stick periods. For comparison, in the same figures we plotted a phase portrait and time realization of the strange attractor at a slightly higher value of parameter α. There are two basic features distinguishing the latter case: First, the ratio of characteristic times is much smaller; second, there is no clear distinction between small and large slipping events. These differences become even more pronounced at larger γ. However, the increase in γ may lead to the destruction of the chaotic regime in the blue-sky catastrophe, which is an inevitable feature in this region of the α-γ plane. It should also be noted that no sharp transition was observed between the two regimes pointed out. Under a decrease in α, the small slipping one-block events become more and more pronounced, which eventually results in a regime with separated time scales. So, from the point of view of dynamical chaos theory the both regimes are one and the same strange attractor.

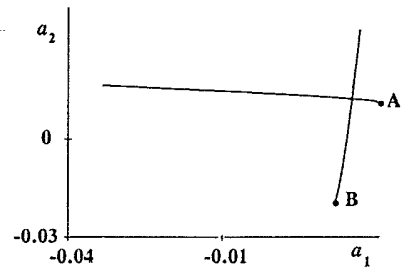

FIG. 15. Graphical solution of algebraic equations (A1) at $g=260.0$, $\alpha=0.015$, $\gamma=20.0$, $\kappa=100.0$, and $\omega_0^2=201.0$.

VI. CONCLUSION

The primary goal of the present work was to elucidate what types of behavior may occur in a mechanical model of faults interaction with two degrees of freedom. We have found that typically there exist a number of periodic, quasiperiodic, and chaotic motions in extended regions of the CPS. The chaotic oscillations were of our particular interest, showing a considerable promise in modeling earthquake activity [31]. It should be stressed that the presence of chaotic motion is typical for the system studied, even in the absence of any spatial inhomogeneity.

A distinctive feature of our study is the modified friction-velocity relation, which, on the one hand, is more realistic than the one used in previous works, since it includes the presence of a creeping motion, and, on the other hand, its form enabled us to perform an analytic investigation of some characteristic oscillatory regimes and to perform well controlled numerical experiments in a large area of the CPS.

The rise of asymmetric periodic attractors was demonstrated to play a key role in the formation of chaotic sets in the phase space. By applying the averaging procedure, we succeeded in getting the approximate appearance condition of the asymmetric motions, thus providing a tool for predicting the rise of chaos associated with this type of attractors.

Extensive numerical experiments have been performed in order to explore the principal features of the behavior. The multistability property is demonstrated to be an important and ubiquitous feature of this system, defining both the sudden and gradual transformations of phase portraits under the change in control parameters. The transitions between attractors with different types of symmetry were also traced and studied in detail.

It follows from both theoretical predictions and numerical simulations that for a certain combination of α and κ, it is possible to find chaotic regimes at almost any value of parameter γ, responsible for the instability rate during the slip phase of blocks motion. Hence the system can produce complicated dynamics with practically any particular form of velocity weakening friction. This

demonstrated not to be the case for the remaining two parameters α and κ. On the contrary, the general properties of motion strongly depend on their magnitudes. The large areas of chaotic dynamics in the CPS as a rule exist when the following approximate relations hold: $\alpha \ll 1$ and $\kappa \cong \omega_0^2/2$. This imposes certain limitations on the corresponding physical parameters of this model. Specifically, the velocity of slow steady motion of the bottom plate in Fig. 1 should be kept small in order to produce chaos. Otherwise only periodic oscillations occur. It is interesting to note that exactly the same behavior was recently reported from the physical experiment with the single spring-block system [32]. It was also shown that in order to produce chaotic regimes with both significantly different time scales of stick and slip phases of motion and well separated magnitudes of slip events, the conditions of small values of α and $g \to \infty$ should be met together with fine-tuned values of the parameter γ.

Note added. After the present paper had been submitted for publication, we became aware of a work [33] where the numerical study of a similar model was performed, but with a different block driving mechanism (train model). Other distinctive features of our study are the usage of analytical methods for predicting the appearance of complex time behavior in the system and the detailed study of bifurcations in a broad range of control parameters variation.

ACKNOWLEDGMENTS

This work was done during the stay of V.B.R. at Meteorological Research Institute. It was supported by the Science and Technology Agency of Japan and the Soros International Science Foundation. We would like to thank Professor J. S. Langer and Professor D. M. Vavriv for fruitful discussions.

APPENDIX

We will show in this appendix how to obtain the inequality (11) from the system of three nonlinear algebraic equations for the coordinates of fixed points of the system (9). Equating the right-hand sides of (9) to zero, rearranging the terms, and taking into account that $a_1^* \neq a_2^*$ and $\theta^* = \pm\pi/2$, where variables with an asterisk are the sought for values, we obtain the following system of equations for the steady state amplitudes:

$$a_1^* = \frac{2\omega_0 a_2^*}{\kappa\pi}\left\{\gamma I(a_2^*) - \frac{g}{2}[\pi - \xi(a_2^*) + \sin\xi(a_2^*)\cos\xi(a_2^*)]\right\},$$
$$a_2^* = -\frac{2\omega_0 a_1^*}{\kappa\pi}\left\{\gamma I(a_1^*) - \frac{g}{2}[\pi - \xi(a_1^*) + \sin\xi(a_1^*)\cos\xi(a_1^*)]\right\}. \quad \text{(A1)}$$

The asymmetric periodic motions with amplitudes a_1^*, a_2^* are expected to exist in the system (7) if algebraic equations (A1) have positive roots. The graphical representation of the solution is given in Fig. 15, where the curves defined by Eqs. (A1) are plotted in the a_1, a_2 coordinates. Their intersection gives the position of the root, whereas the absence of the intersection means that there exist no asymmetric fixed points in (9) and no associated limit cycles in (8). The points A and B on this plot correspond to the cases $a_1^* = -v_0$ for the first and the second equations of (A1), respectively, and their position can be obtained by substituting the value of v_0 into (A1) and noticing that $\xi(-v_0) = \pi$,

$$A = (W_0, -v_0), \quad B = (-v_0, -W_0). \quad \text{(A2)}$$

Numerical experiments indicate that under variation of the control parameters, the only way for the root to disappear is by moving point A to the left of the second curve. Thus the borderline in the CPS enclosing the region of asymmetric attractors existence is defined by the condition that A belongs to both of the curves pointed out. Calculating the value of W_0 from the second equation of (A1) and substituting it into the first leads to the relation (11).

[1] T. Cao and K. Aki, PAGEOPH **122**, 10 (1984).
[2] J. R. Rice and S. T. Tse, J. Geophys. Res. **91**, 521 (1986).
[3] J. M. Carlson, J. Geophys. Res. **96**, 4255 (1991).
[4] J. M. Carlson and J. S. Langer, Phys. Rev. A **40**, 6470 (1989).
[5] J. M. Carlson, J. S. Langer, and B. E. Shaw, Rev. Mod. Phys. **66**, 657 (1994).
[6] J. M. Carlson, J. S. Langer, B. E. Shaw, and C. Tang, Phys. Rev. A **44**, 884 (1991).
[7] S. L. Pepke and J. M. Carlson, Phys. Rev. E **50**, 236 (1994).
[8] S. L. Pepke, J. M. Carlson, and B. E. Shaw, J. Geophys. Res. **99**, 6769 (1994).
[9] B. E. Shaw, J. M. Carlson, and J. S. Langer, J. Geophys. Res. **97**, 479 (1992).
[10] H. Nakanishi, Phys. Rev. A **46**, 4689 (1992).
[11] J. Schmittbuhl, J.-P. Vilotte, and S. Roux, Europhys. Lett. **21**, 375 (1993).
[12] P. Espanol, Phys. Rev. E **50**, 227 (1994).
[13] K. Christensen and Z. Olami, J. Geophys. Res. **97**, 8729 (1992).
[14] B. Lin and P. L. Taylor, Phys. Rev. E **49**, 3940 (1994).
[15] A. Crisanti, M. H. Jensen, A. Vulpiani, and G. Paladin, Phys. Rev. A **46**, R7363 (1992).
[16] H. Nakanishi, Phys. Rev. A **43**, 6613 (1991).
[17] M. de Sousa Vieira, Phys. Rev. A **46**, 6288 (1992).
[18] M. de Sousa Vieira, G. L. Vasconcelos, and S. R. Nagel, Phys. Rev. E **47**, R2221 (1993).
[19] J. Nussbaum and A. Ruina, PAGEOPH **125**, 629 (1987).
[20] J. Huang and D. L. Turcotte, PAGEOPH **138**, 569 (1992); Geophys. Res. Lett. **17**, 223 (1990); Nature **348**, 234 (1990).
[21] D. G. Aronson, E. J. Doedel, and H. G. Othmer, Physica

D **25**, 20 (1987).
[22] D. G. Aronson, G. B. Ermentrout, and N. Kopell, Physica D **41**, 403 (1990).
[23] N. N. Bogoliubov and Yu. A. Mitropolsky, *Asymptotic Methods in the Theory of Nonlinear Oscillations* (Gordon and Breach, New York, 1961).
[24] V. B. Raybov and D. M. Vavriv, Phys. Lett. A **153**, 431 (1991).
[25] F. Heslot, T. Baumberger, B. Perrin, B. Caroli, and C. Caroli, Phys. Rev. E **49**, 4973 (1994).
[26] I. Pastor, V. M. Perez-Garcia, F. Encinas-Sanz, and J. M. Guerra, Phys. Rev. E **48**, 171 (1993).
[27] M. Poliashenko and S. R. McKay, Phys. Rev. A **44**, 3452 (1991).
[28] *Chaotic Oscillators: Theory and Applications,* edited by T. Kapitaniak (World Scientific, Singapore, 1992).
[29] A. Wolf, J. B. Swift, H. L. Swinney, and J. A. Vastano, Physica D **16**, 285 (1985).
[30] J. F. Heagy, T. L. Caroll, and L. M. Pecora, Phys. Rev. E **50**, 1874 (1994).
[31] *Nonlinear Dynamics and Predictability of Geophysical Phenomena,* edited by W. I. Newman, A. Gabrielov, and D. L. Turcotte, AGU Geophysical Monograph No. 83 (IUGG, Washington, DC, 1994), Vol. 18.
[32] A. Johansen, P. Dimon, C. Ellegaard, J. S. Larsen, and H. H. Rugh, Phys. Rev. E **48**, 4779 (1993).
[33] M. de Sousa Vieira, Phys. Lett. A **198**, 407 (1995).